Khagendra Tripathi[1]
Metals and Materials Engineering Department,
Sun Moon University,
100, Kalsan-ri,
Asan 336-708, South Korea
e-mail: tripathikhagendra25@gmail.com

Bhupendra Joshi
Metals and Materials Engineering Department,
Sun Moon University,
100, Kalsan-ri,
Asan 336-708, South Korea
e-mail: joshibhupen@gmail.com

Gobinda Gyawali
Metals and Materials Engineering Department,
Sun Moon University,
100, Kalsan-ri,
Asan 336-708, South Korea
e-mail: gbngyawali@gmail.com

Auezhan Amanov
Mechanical Engineering Department,
Sun Moon University,
100, Kalsan-ri,
Asan 336-708, South Korea
e-mail: amanov_a@yahoo.com

Soo Wohn Lee[1]
Metals and Materials Engineering Department,
Sun Moon University,
100, Kalsan-ri,
Asan 336-708, South Korea;
Environmental Engineering Department,
Sun Moon University,
100, Kalsan-ri,
Asan 336-708, South Korea
e-mail: swlee@sunmoon.ac.kr

A Study on the Effect of Laser Surface Texturing on Friction and Wear Behavior of Graphite Cast Iron

Dimples with various pitches and densities were produced using laser surface texturing (LST) to improve the friction and wear behavior of graphite cast iron. The objective of this study is to investigate the effectiveness of dimples on the friction and wear behavior of an internal combustion engine (ICE) cylinder. The specimens with a dimple pitch of 150 μm and a dimple density of 13% exhibited the lowest friction coefficient among the specimens, while the specimens with a dimple pitch of 200 μm and a density of 7% exhibited the highest resistance to wear. [DOI: 10.1115/1.4030859]

Introduction

Over the years, a number of efforts have been made to save energy waste due to the friction between the mechanical components of ICEs. Friction loss is considered a prominent factor which determines the fuel efficiency and performance of a vehicle. An energy loss of about 50% is associated with the piston/cylinder system. A number of efforts had been made earlier to reduce this friction loss and are still continuing. It is well known that surface structure has a significant influence on the friction, wear, and lubrication performance of ICEs [1–3]. Creating designs with suitable roughness parameters instead of a perfectly smooth surface leads to a low friction and wear of the mechanical components [3]. Surface engineering is a well-known method for improving the tribological properties of engine components [4–6]. Among all the practical surface modification methods, LST seems to be the most promising because of its extremely fast speed and environmental friendliness. It also provides an excellent control over the shape and size of the microdimples, which allows the realization of optimal designs. Indeed, LST has already attracted a lot of attention in the Tribology community, as evident from the growing number of publications on this topic. It has been found to be beneficial to improving the friction and wear behavior of mechanical components owing to its applicability and to the possibility of creating microdimples, channels, and grooves on the surface of various materials. It has been reported earlier that the friction and wear behavior can be minimized by the introduction of selective microdimples on sliding surfaces [7–16]. Several mechanisms have been proposed to explain the influence of dimples, grooves, channels, and/or patterns made by LST on the tribological properties [17]: (a) they can serve as microhydrodynamic bearings to generate additional hydrodynamic pressure to provide additional lift, (b) they might act as lubricant microreservoirs, as a secondary source of lubricant for enhancing lubricant retention, (c) they can provide an easier escape for the wear debris generated by reducing the third-body abrasion, and (d) they reduce the contact area of mating surfaces in relative motion. According to the studies, microdimples can create microtraps for wear debris in lubricated and/or dry sliding, microreservoirs for lubricant in the case of starved lubrication conditions, and microhydrodynamic bearings in the case of full or mixed lubrication [18–22]. Thus, the textured specimen helps to increase the oil film thickness between the mated surfaces in such a way that transitions from the boundary lubrication regime to a mixed lubrication regime and then into a hydrodynamic regime occur [23,24]. Hence, it reduces the friction generation between the surfaces in relative motion. In addition, closed microcavities, like small circular pits, can perform the function of hydrostatic microbearings [5]. In fact, the fluid in the cavities becomes compressed and produces a bearing pressure when two mated surfaces come close to each other during

[1]Corresponding authors.

Contributed by the Tribology Division of ASME for publication in the JOURNAL OF TRIBOLOGY. Manuscript received December 5, 2014; final manuscript received April 9, 2015; published online August 6, 2015. Assoc. Editor: Daniel Nélias.

Table 1 Chemical composition of cast iron specimen analyzed by energy dispersive X-ray analysis

Elements	C	Si	P	S	Cr	Mn	Ni	Cu
wt. %	2.47 ± 0.16	0.43 ± 0.05	≤0.06	≤0.05	0.45 ± 0.08	1.03 ± 0.11	≤0.06	≤0.1

sliding. The kind of structures, geometry, and the density of the cavities on the flat surface play an important role in controlling the tribological properties. In most cases, an optimized structure can only be achieved if it adapts to the tribological system.

The specimens from an ICE cylinder are modified by creating hemispherical dimples on the surface by LST. Since the size, shape, and distribution of the dimples produce a preliminary effect on both the friction [21,25] and Stribeck curve in lubricated sliding [26], the dimple density was quantified using the following expression:

$$\text{dimple density} = \frac{\pi d_d^2}{4S^2} \times 100\% \tag{1}$$

where d_d is the dimple diameter, S is the dimple pitch.

Many researchers have explored the beneficial effects of LST on reduction in the friction of piston rings, but a very few have worked on the cylinder liner. In this regard, it is interesting to observe the effects of LST on the friction and wear behavior of a cylinder liner made of cast iron. Several issues exist in the LST application on piston–cylinder systems because the dimple parameter selection for LST is a difficult task. Also, the dimple pitch/density should be correlated with the roughness parameters of the specimens that effect on the tribological behavior.

This study reports not only the beneficial effect of texturing on the reduction of friction and wear but also recognizes the importance and effectiveness of roughness parameters following a change of dimple pitch/density.

Experimental Procedure

Sample Preparation. Specimens with dimensions of $15 \times 15 \times 4$ mm^3 were prepared from an ICE cylinder. The chemical composition of the specimens employed in this study is shown in Table 1. The specimens were ground for flatness using a grinding machine and then mirror polished using alumina suspension down to a particle size of 1 μm. The hardness of the polished cast iron specimen was about 225 HV. The average roughness (R_a) of a polished specimen was about 0.0115 μm. The specimens were then subjected to LST.

LST. LST was performed on the polished specimens using laser radiation of a wavelength of 1064 nm (INYA −20 W, Germany). The laser radiation was operated with a pulse width of 200 ns and a frequency of 20 kHz to produce hemispherical dimples. The laser beam was focused onto the specimens by an objective lens (focal length, $f = 323$ mm) and scanned over the surface via deflection mirrors.

The LST was conducted with a variation of dimple pitch and density to investigate its effects on friction and wear. Dimple dimensions with a diameter of about 58–60 μm and a depth of about 28–30 μm were produced on the specimen where the aspect ratio was found to be 0.5. As-prepared textured specimens are referred to as S80, S100, S150, and S200 for the specimens with a dimple pitch of 80, 100, 150, and 200 μm, respectively.

The ablated materials were removed using an air gun during the laser process. However, all the specimens after laser ablation were repolished gently to remove the molten debris accumulated on the surface. Prior to testing, the specimens were cleaned with ethanol for 10 mins in an ultrasonic bath.

Friction and Wear Test. Friction and wear tests were carried out using a ball-on-disk (CSM Instruments, Switzerland) tribometer at a normal load of 10 N and a speed of 0.05 m/s under unidirectional sliding with a rotation radius of 3 mm. A bearing steel (SAE52100) ball with a diameter of 12.7 mm was used as a counter surface. The corresponding Hertzian contact pressure was about 0.79 GPa. The effect of load (5–15 N) and speed (0.005–0.05 m/s) variations on the friction coefficient was also studied on a textured specimen. The tests were conducted with the sliding time of 60 min and the sliding length of 180 m at room temperature with a relative humidity of 25–30%.

The influence of different dimple pitch/density on the tribological performance was assessed under oil-lubricated conditions. The specimens were fully immersed in lubricants (engine oil, 5W30 Exxon Mobil Oil Corp., Fairfax, VA) during the friction tests. The physical properties of the oil were listed in Table 2.

Surface Analyses. All the specimens before and after LST were observed and investigated carefully using an optical microscopy (OM). Generated wear tracks on the disk specimens and wear scars on the balls were observed by a large-scaled measuring microscope (Model-STM6-LM-F31-2, Japan). The surface morphology and dimples were observed using a mini-SEM (Nanoeye, SNE-3000 M, South Korea). The roughness parameters, such as average roughness (R_a), average peak to valley height (R_z), skewness (R_{sk}), and kurtosis (R_{ku}), of the specimens were measured before and after LST, and cross-sectional dimple profiles were also obtained using a surface profilometer (Surftest SV-600, Japan). The wear volume of the specimens was analyzed by plotting wear track profiles. The actual wear volume of the textured surfaces was quantified by deducting the area of dimples inside the wear track. The wear volume of the ball was calculated using the following equation:

$$V_{ball} = \frac{\pi h}{6}\sqrt{\frac{3d_w^2}{4} + h^2} \tag{2}$$

where d_w is the wear scar diameter, and h is the height of the worn out part of the ball which is related to the radius (r) of the ball as

$$h = r - \sqrt{r^2 - \frac{d_w^2}{4}} \tag{3}$$

The specific wear rate of the ball and the disk specimens was calculated using the following equation:

$$W = \frac{V}{N \cdot l} \tag{4}$$

where V is the wear volume, N is the normal load applied, and l is the total sliding distance.

Table 2 Physical properties of lubricant oil

Lubricant oil	
Society of Automotive Engineers (SAE) grade	5W30
Density	0.855 g/l
Pour point	−42 °C
Flash point	230 °C
Viscosity (at 40 °C)	61.7 cSt
Viscosity (at 100 °C)	11 cSt

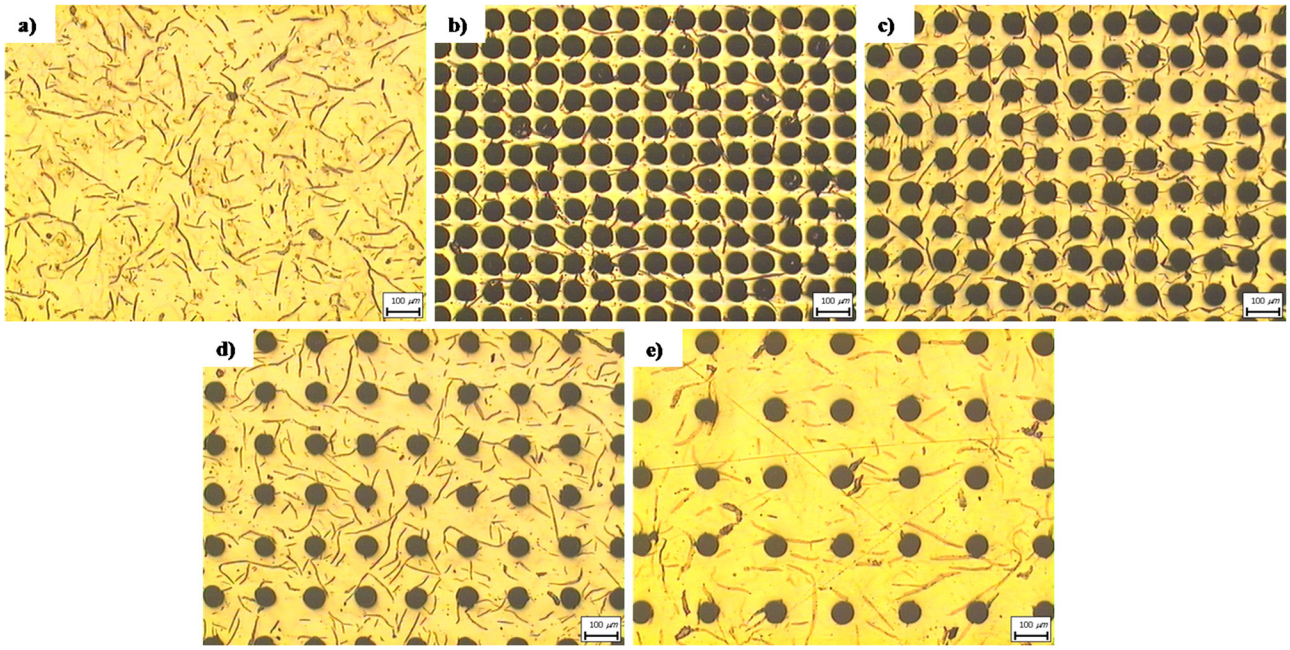

Fig. 1 OM images of untextured and textured specimens before friction test: (*a*) untextured, (*b*) S80, (*c*) S100, (*d*) S150, and (*e*) S200, respectively

Results and Discussion

Surface Topography. Figure 1 shows the OM images of the untextured and textured specimens. It can be seen that the graphite flakes were uniformly distributed over the surface. It has been reported earlier that the graphite flakes are responsible for the reduction in the friction coefficient for the untextured specimen, since graphite acts as a lubricious material at room temperature [27]. Uniformly distributed circular dimples with a square pattern are observed on textured specimens with various dimple pitches/densities. Figures 2 and 3 are the cross-sectional images of a dimple and the dimple profiles of the textured specimens, respectively. It is obvious from Fig. 2 that the depth of the dimples was about 30 μm. Figure 3 corresponds to the profiles of various textured specimens with different dimple pitch/density. It also describes the dimple dimensions, such as the dimple diameter, the dimple depth, and the dimple pitch. The surface characteristics of the textured specimens employed for the friction and wear tests are presented in Table 3. With the various dimple pitch/density of the textured specimens, a change in the roughness parameters was noticed. The roughness parameters of the textured specimens before the friction and wear test are presented in Table 4. The S150 specimen exhibited the lowest R_a and R_z values among all the textured specimens. A smaller R_z value corresponds to a smoother surface and leads to low friction and long life. The R_z value of the textured specimens seems to be nearly equal to the dimple depth obtained through the cross-sectional scanning electron microscopy (SEM) image. This is mainly because of the subtle peak heights, as compared to the valley depths, after laser ablation. If the R_z values are compared among the textured specimens, a little variation can be seen in the R_z value, which is due to the laser power deviation. As shown in Table 4, dimple pitch showed a considerable effect on both the R_{ku} and R_{sk} values. It was noted that R_{ku} increased, and R_{sk} changed toward a more negative value with increasing dimple pitch, from 80 to 150 μm. A further increase in dimple pitch up to 200 μm resulted in a

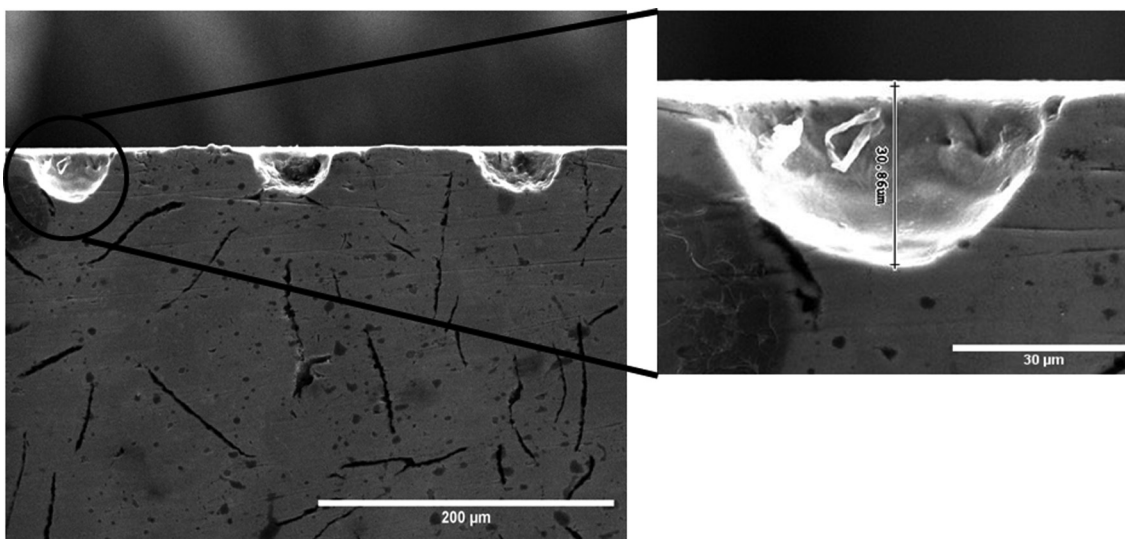

Fig. 2 SEM image of cross section of a dimple created on the cast iron specimen

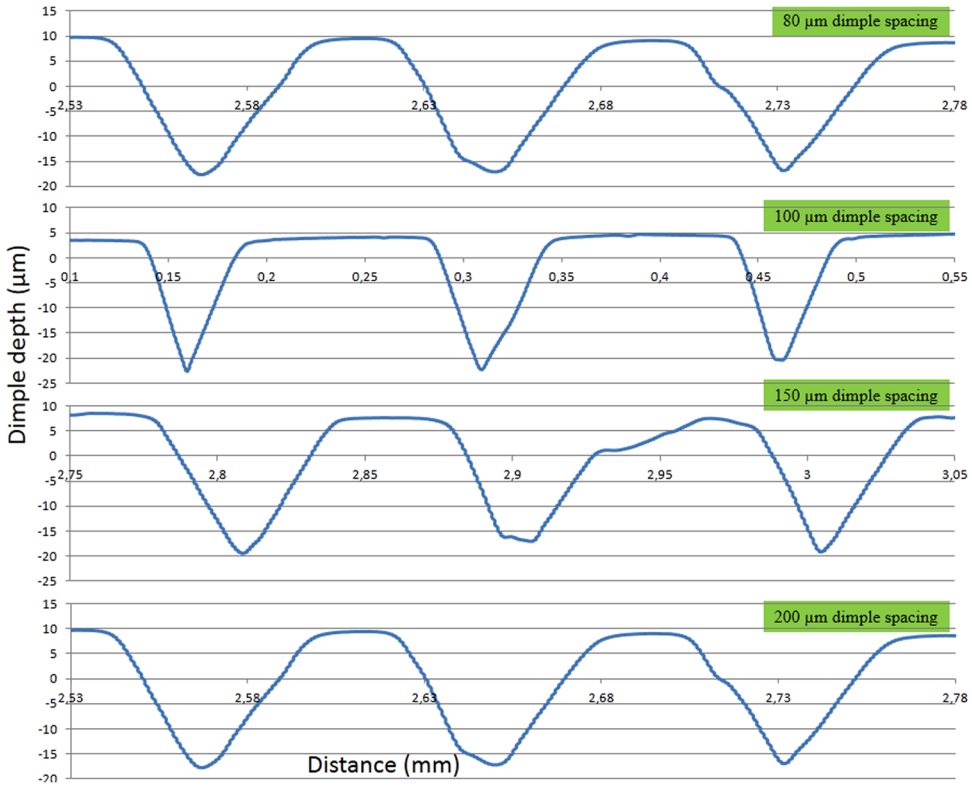

Fig. 3 Profiles of dimples on textured specimens

Table 3 Surface characteristics of textured specimens employed for friction and wear test

	Specimens			
Dimple parameters	S80	S100	S150	S200
Average dimple diameter (μm)	58–60	58–60	58–60	58–60
Dimple depth (μm)	25–30	25–30	25–30	25–30
Dimple density (%)	44	28	13	7
Dimple pitch (μm)	80	100	150	200

Table 4 Roughness parameters of textured specimens

	Roughness parameters			
Textured specimens	R_a (μm)	R_{sk}	R_{ku}	R_z (μm)
S80	3.740	−0.599	3.873	26.512
S100	3.328	−1.245	5.720	26.567
S150	2.320	−2.191	10.549	25.332
S200	3.061	−2.188	8.835	26.771

decrease in R_{ku}, and changed R_{sk} to a lesser negative value. The small effect of this change on R_{sk} and R_{ku} values is because of the wall inclination of the dimples on the specimens, but the significant effect is due to the alteration of the surface topography by dimple pitch variation.

The third- and fourth-order central moment R_{sk} and R_{ku} values were measured to obtain more information about the real profile form of the textured specimens. R_{sk} evaluates the degree of asymmetry in cases of asymmetric distribution, whereas R_{ku} describes the distribution sharpness. $R_{sk} = 0$ and $R_{ku} = 3$ represent the Gaussian distribution of a surface. It is a significant parameter for tribological applications, such as bearing surface functionality, wear control, and others [28]. On the other hand, the surface with $R_{ku} > 3$ is dominated by sharp peaks (spiky), whereas the surface with $R_{ku} < 3$ is comprised of bumpy peaks. In this regard, information on the real contact area and on its resistance to wear was provided.

All the roughness parameters mentioned above are two-dimensional parameters, which characterize the surface features of the textured specimens. The two-dimensional parameters provided in this study are believed to be sufficient to shed light on the dimple pitch effect on the friction behavior. A significant variation in roughness parameters can be observed between the untextured and textured specimens. Even the roughness of the untextured specimen is found to be negligible compared to the dimple features, and these small changes in roughness parameters due to an increase in dimple pitch are responsible for controlling the friction coefficient. Hence, it can be concluded that the change in roughness parameters can play an important role in the study of the friction and wear behavior of dimpled specimens.

Friction Coefficient. Figure 4 shows the variation in the friction coefficient as a function of sliding time for the untextured and textured specimens. It can be seen that the friction coefficient decreased significantly for the textured specimens when compared to those of the untextured specimens. However, the textured specimen with a dimple pitch of 80 μm led to a higher friction coefficient than that of the untextured specimen. An interference of closely spaced dimples might occur on the highly dense textured specimen (S80) and an adverse effect in the reduction of friction resulted. It also depicts the influence of dimple pitch/density on the friction coefficient of the textured specimens. It shows a variation of the friction coefficient among the textured specimens with various dimple pitches/densities. It is obvious that all the specimens showed the same trend of friction behavior where, at the initial stage of sliding, the friction coefficient increased with increasing sliding time, and finally stabilized to a certain value of the friction coefficient. The increase in the friction coefficient at the initial stage occurred during the running-in period of sliding. The running-in friction coefficient occurs when extrusions and/or

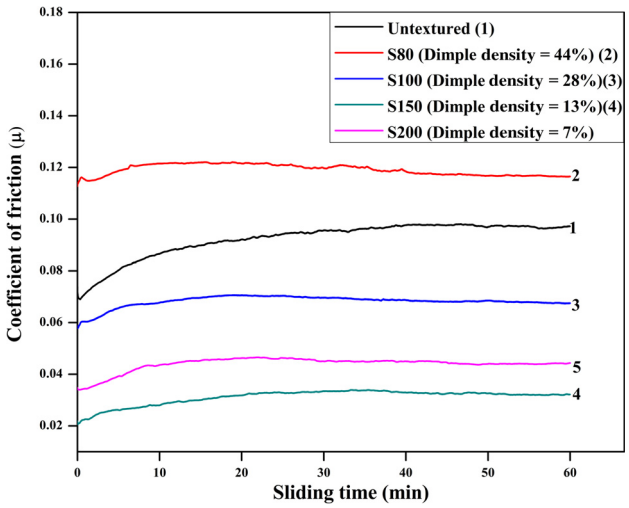

Fig. 4 Variation of friction coefficient untextured and textured specimens as a function of sliding time

protrusions of mated surfaces come into contact during the initial stage of sliding. As the extrusions or/and protrusions on contact surfaces first come into contact, the friction coefficient increases until the contact area increases with the removal of those rougher protrusions or/and extrusions. Once it exceeded the run-in time, the friction coefficient became almost stable. The specimen S150 exhibited the lowest friction coefficient among all the specimens, which is a ~70% reduction in friction compared to that of the untextured specimen. Similarly, the friction coefficient of the specimens S100 and S200 reduced by about ~32% and ~53%, respectively.

The reduction in the friction coefficient for the S150 specimen can be explained in several ways: first, an average surface roughness can be introduced to explain the higher friction coefficient of highly dense textured specimens and the lowest friction coefficient for an optimum textured specimen. Rough surfaces usually produce a higher friction coefficient under lubricated systems, particularly with soft metals, where lubricant films are very thin, compared to the asperity height. If the density of dimples is too high, dimple edges interference occurs, resulting in a higher average roughness and a higher friction coefficient. So, it must be ensured that dimple density will not increase average roughness; rather it should be decreased. Highly dense dimples on a specimen correspond to higher roughness and lead to an increase in the friction coefficient. As per our experimental results, the specimen with a dimple density of 13% is the optimized and the best for the least value of the friction coefficient. Certainly, one of the parameters is the diameter of the counter ball or the contact area in determining the suitable roughness. Another parameter is the number of dimples at the contact interface; second, the variation in the friction coefficient among the textured specimens can be analyzed on the basis of the roughness parameters, such as R_{sk} and R_{ku}. According to the surface roughness analysis, it has been revealed that the reduction in dimple density results in a surface topography with higher R_{ku} and more negative R_{sk} values and consequently, less friction. Thus, an increase in R_{ku} and a more negative R_{sk} leads to a reduction in the friction coefficient in lubricated tests [29]; third, dimples with high density on the specimens will result in a more reduced contact area, increased contact pressure, unfavorable R_{ku} and R_{sk} values, and a negative effect on the friction. Podgornik et al. have reported earlier that the texturing has a detrimental effect on friction if the texturing is not employed with the most favorable parameters [30]. Therefore, the optimum texturing parameters are required to obtain a low friction coefficient. The increase in R_{ku} and negative R_{sk} yield a lower friction coefficient for low load, low-sliding speed conditions. Furthermore, textured specimens with higher R_{ku} and more negative R_{sk} tend to shift the Stribeck curve downwards and to the left, thus reducing the dependence on sliding speed [31]. The lowest friction coefficient was achieved with the S150 specimen, which may be attributed to the higher R_{ku} and more negative R_{sk} compared to the other textured specimens. The dimple density should be kept low so as not to make a considerable effect on the contact-pressure distribution. An increase in R_{ku} and the increase in more negative R_{sk} have been observed in specimen S150, having an optimum dimple density of 13% (see Table 4). Hence, the most significant roughness parameters are skewness and kurtosis in order to obtain a lower friction coefficient of the textured specimens. The higher friction coefficient of the S80 specimen (44% dimple density) was mainly due to several factors, such as unfavorable roughness parameters, higher average surfaces, contact-pressure distribution, and dimple edges interference on the contacting surfaces. A pressure build-up will be created by the dimple edge, and the pressure build-up depends on the total number of dimple edges in the contact area. Kovalchenko et al. have reported that a lower friction exhibited with higher packing density on two surfaces with a 7% and 14% dimple density [32]. For a higher textured area, more dimple edges in contact create a higher pressure build-up. However, dimples with a high density are equivalent to less contact area and high contact pressure; they also might create interference resulting in a higher friction coefficient.

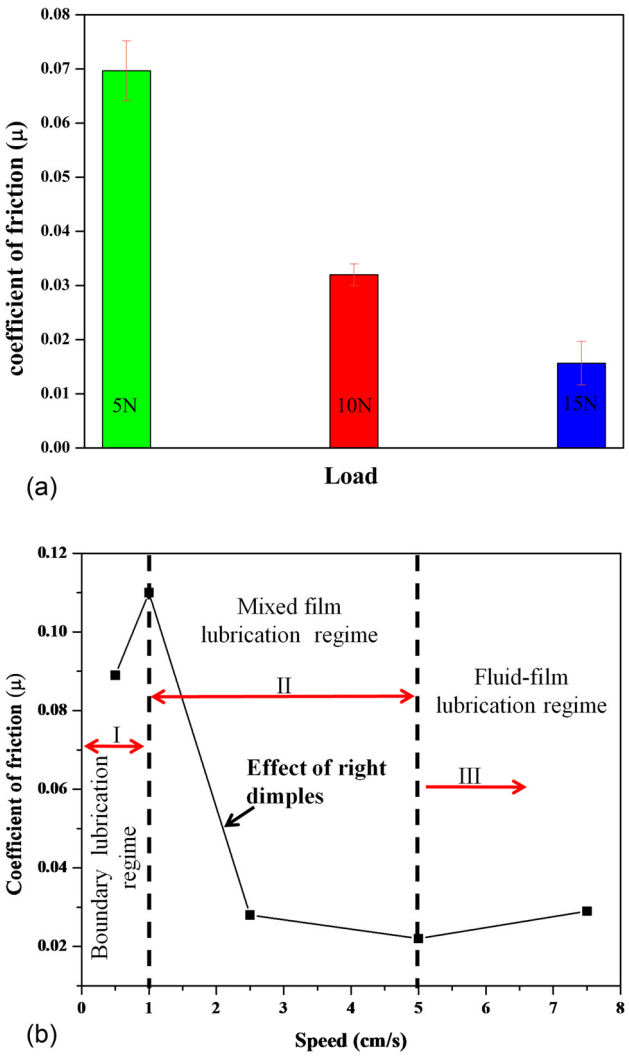

Fig. 5 Effect of (*a*) normal load and (*b*) sliding speed on friction coefficient of specimen S150

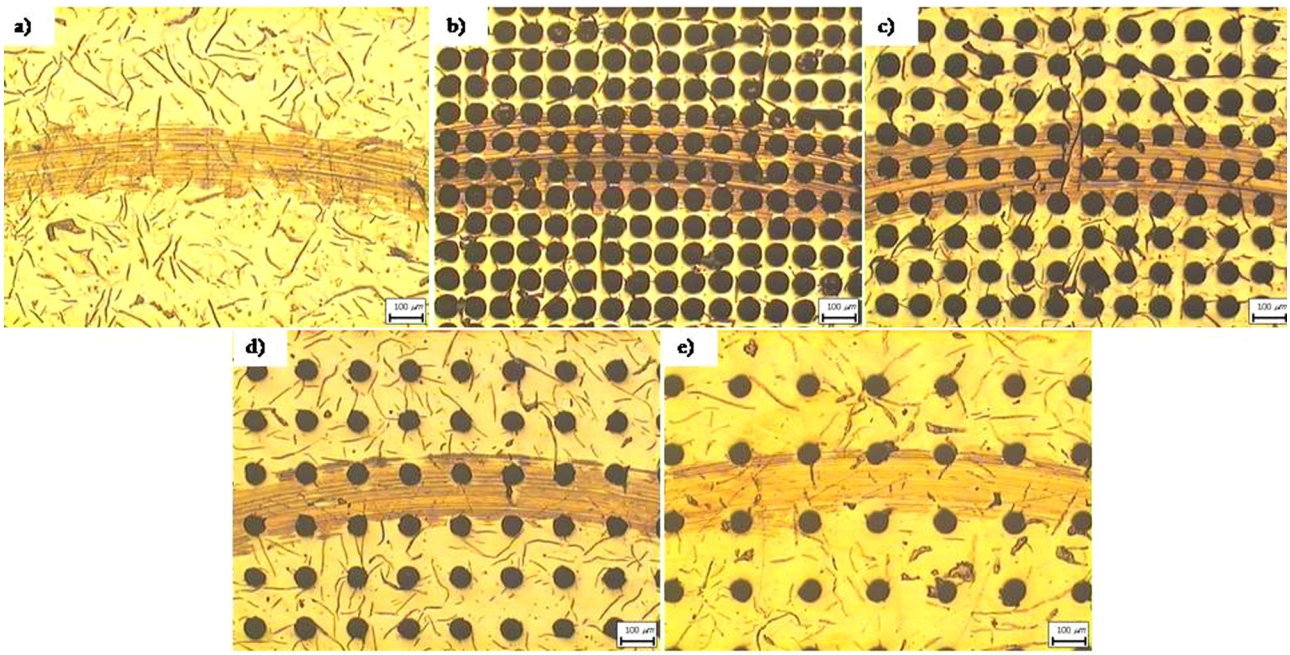

Fig. 6 Optical images of wear tracks on untextured and textured specimens: (*a*) untextured, (*b*) S80, (*c*) S100, (*d*) S150, and (*e*) S200, respectively

Load and Speed Effect on Friction Coefficient. Almost all operating parameters (speed, load, etc.) will have an effect on the friction coefficient of mechanical parts, as they change the sliding conditions. In this study, the effects of load and speed on friction behavior were investigated on textured specimens. Specimen S150 was selected to be investigated, since it exhibited the lowest friction coefficient among the textured specimens. Figure 5(*a*) shows the effect of load on the friction coefficient at a fixed speed of 0.05 m/s. It can be seen that the friction coefficient of the textured specimen reduced by increasing the normal load. A large quantity of wear debris and smoothing phenomena are believed to be responsible for the reduction in friction by increasing the normal load [33,34]. Hence, the beneficial effect of higher loads on the reduction in the friction coefficient of the S150 specimen was investigated for higher loads. Figure 5(*b*) shows the effect of sliding speed on the friction coefficient at a fixed normal load of 10 N. It is obvious from Fig. 5(*b*) that the friction coefficient increased and then decreased with increasing sliding speed. An

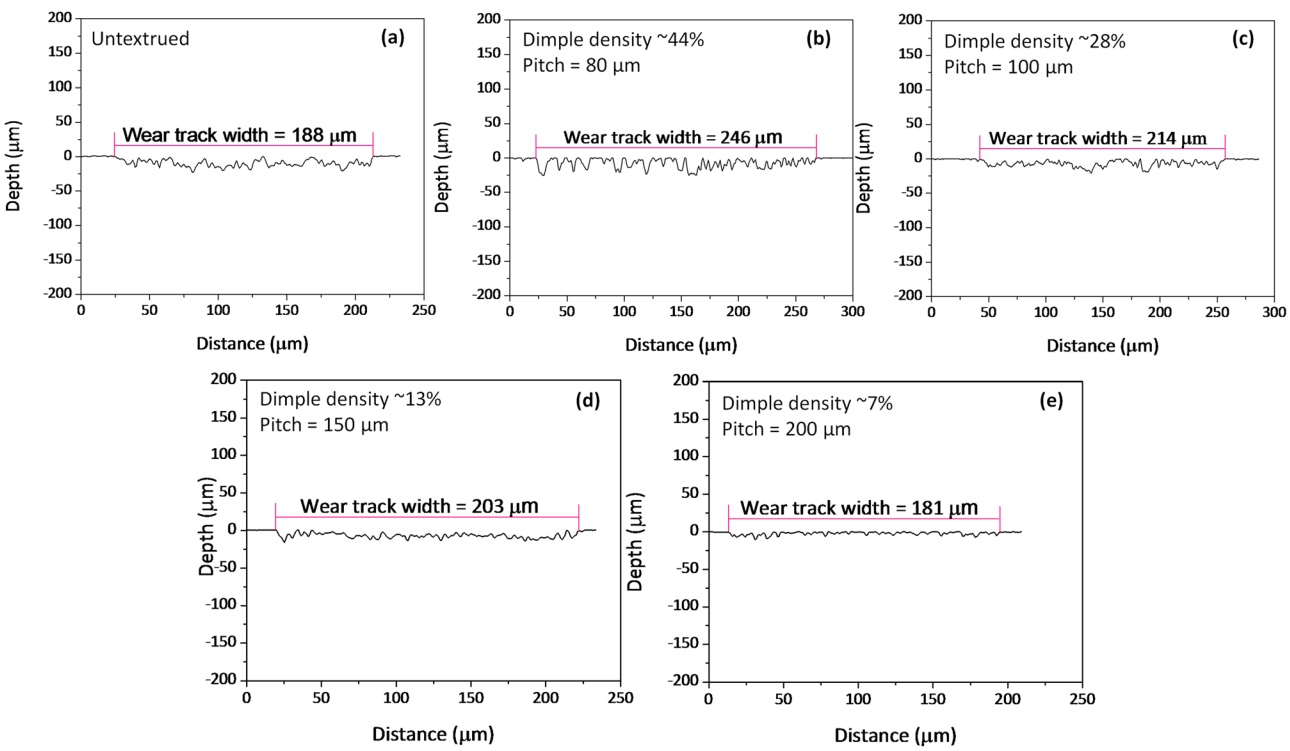

Fig. 7 Wear track profiles of untextured and textured specimens: (*a*) untextured, (*b*) S80, (*c*) S100, (*d*) S150, and (*e*) S200

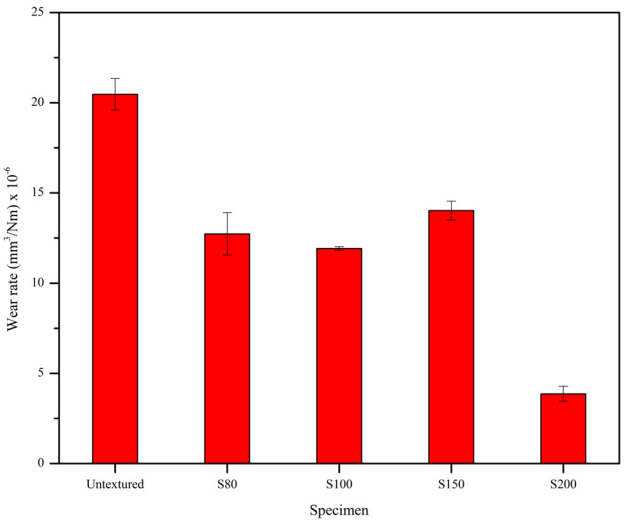

Fig. 8 Wear rate of untextured and textured specimens

increase in speed decreases wear because of the generation of micro-elastohydrodynamic lubrication (EHL) films and the reduced chance of squeezing the surface film between colliding asperities. The shearing of metals decreases as the speed increases and reaches very low values. Due to the occurrence of low sharing at higher speed, the mated surfaces never come into contact. Actually, it is beneficial for the increment of the oil film thickness. This variation of shearing between surfaces in contact at different speeds alters the oil film thickness, which is helpful in the transition of the lubrication regime. As the speed increases, the transition takes place from the boundary lubrication regime to a mixed lubrication regime, and at last transits to a fluid film lubrication regime. In fact, a reduction in the friction coefficient resulted within region II under a mixed lubrication regime. As shown in Fig. 5(*b*), there are three lubrication regimes: (1) the boundary lubrication regime; (2) the mixed film lubrication regime; and (3) the hydrodynamic lubrication regime. At low speeds, a thin lubricant film increases the shearing of surfaces, which occurs between the contact specimens. The lubrication film had little effect, and the friction coefficient of the specimen will be higher. As the speed increases further, the effect of the hydrodynamic pressure generated on the surface by dimples lift the specimen, and shearing between contact surfaces becomes smaller, and the friction coefficient decreases. At this stage, an extensive interaction of surface materials occurs, and the mixed film plays the significant role in decreasing the friction coefficient. By increasing sliding speed further, another stage occurs, at which the lowest friction coefficient results. Afterward, the friction coefficient again rises, due to the large amount of hydrodynamic pressure and a negligible sharing of surfaces. In this case, the contacting surfaces are mainly separated by the lubricant fluid film, and the friction is governed completely by the shearing of the lubricant fluid film dependent on the rheological properties of a lubricant.

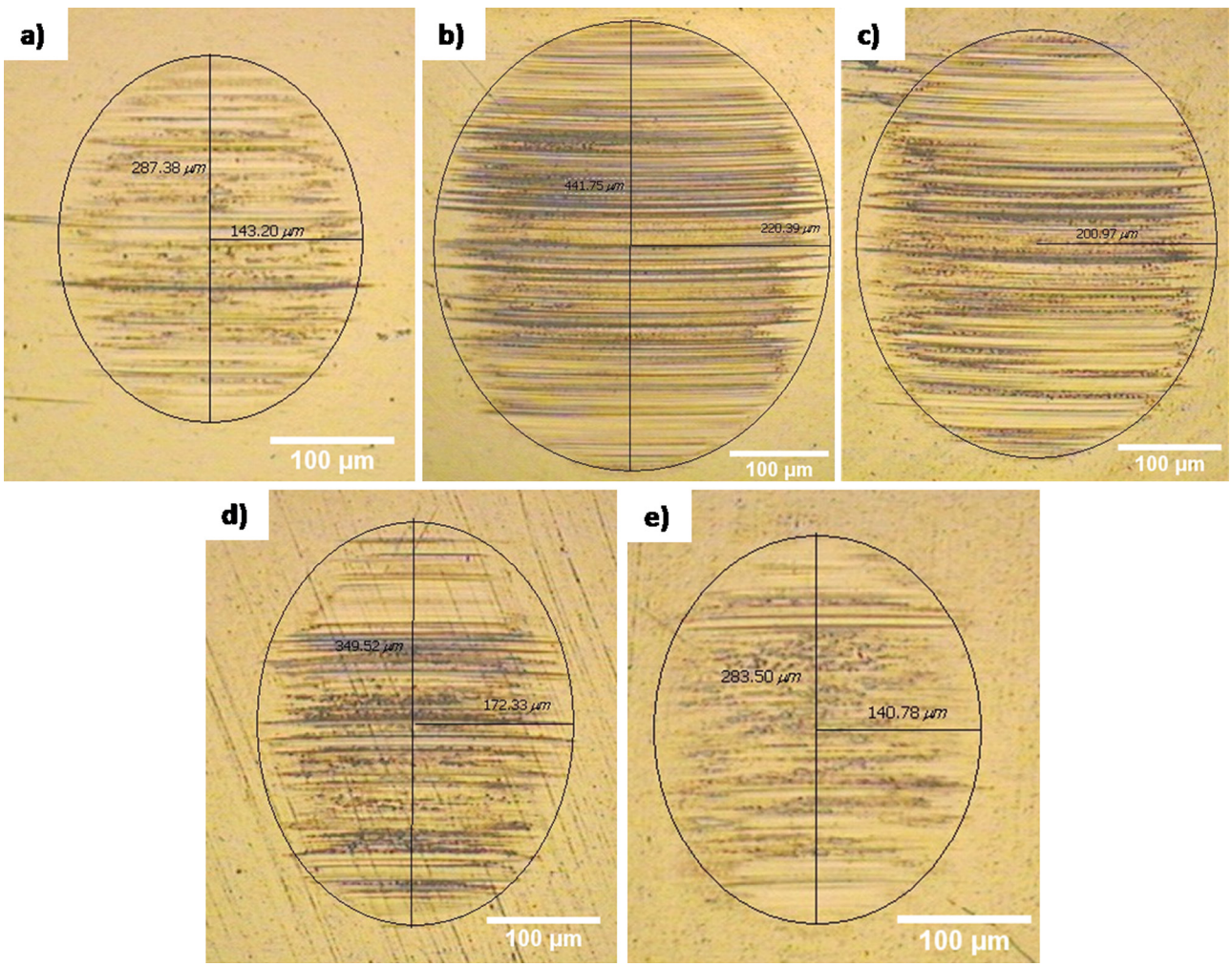

Fig. 9 Optical images of wear scar developed on steel balls slid against: (*a*) untextured, (*b*) S80, (*c*) S100, (*d*) S150, and (*e*) S200, respectively

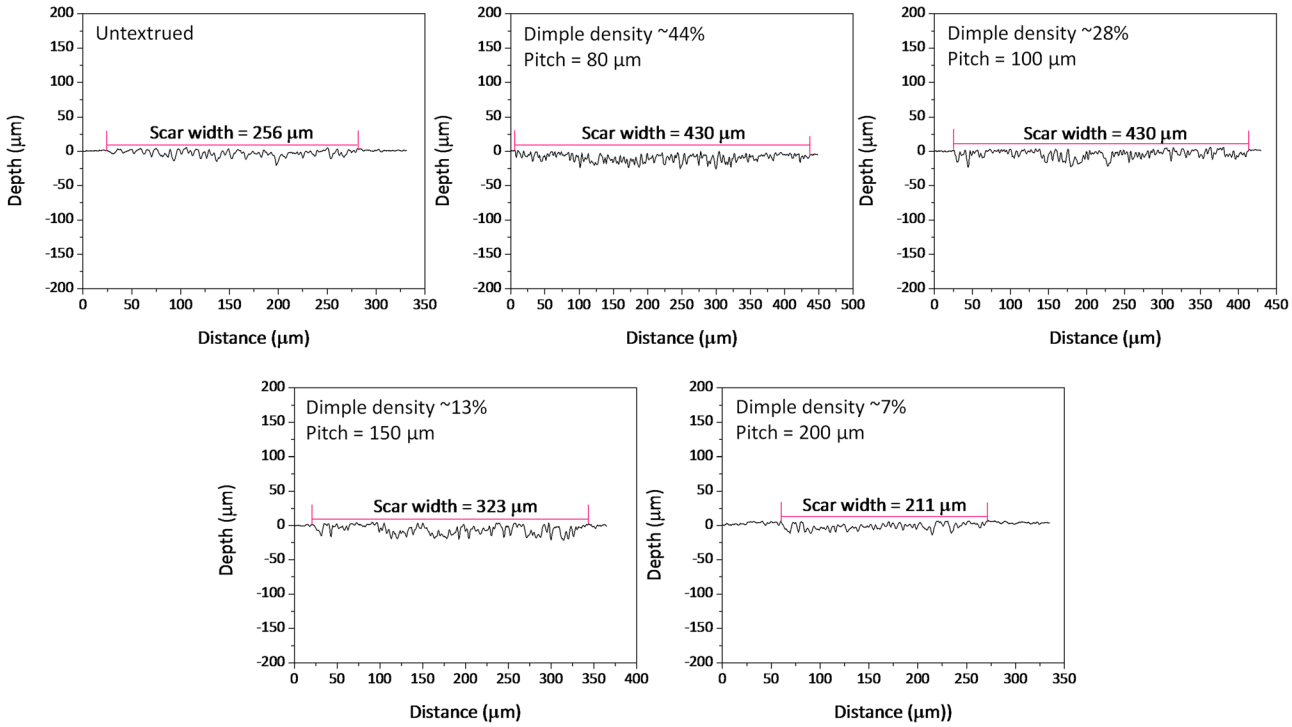

Fig. 10 Ball scar wear profiles slid against untextured and textured specimens

Wear Analysis. Figure 6 shows the OM images of wear tracks observed on the untextured and textured specimens. It is clear that the presence of dimples inside the wear track on the textured specimens reduced the real contact area and decreased the actual worn surfaces. Thus, deducing the textured area inside a wear track gives the actual worn out part of the textured specimen. This theory was used to calculate the wear volume of the textured specimens. Wear profiles of the untextured and textured specimens are presented in Fig. 7. It can be seen that the S80 specimen exhibited a slightly wider and deeper wear track in comparison to the untextured specimen. However, the S100 specimen had a comparable width and shallower wear profiles. The S150 and S200 specimens showed narrower, and shallower wear profiles compared to that of the untextured specimen. Obviously, the S80 specimen had a higher roughness among the other textured specimens, which resulted in wider and deeper wear track. All the wear profiles of the textured specimens were measured on the untextured regions of wear tracks.

Figure 8 presents the wear rate of the untextured and textured specimens. The wear rate of the untextured specimen was found to be 20.7×10^{-6} mm^3/N·m, while the wear rate was found to be $\sim 11.7 \times 10^{-6}$, $\sim 11.9 \times 10^{-6}$, $\sim 14.5 \times 10^{-6}$, and 3.4×10^{-6} mm^3/N·m for the S80, S100, S150, and S200 specimens, respectively. The wear rate of the textured specimens decreased by about 43%, 42.5%, 30%, and 84% for the S80, S100, S150, and S200 specimens, respectively. Though the wear profile of the S80 specimen was wider and deeper, the wear rate decreased, which is mainly due to the presence of a large number of dimples inside the wear track. The same was the case for the S100 and S200 specimens. However, the S200 specimen had a less densely textured surface in comparison to the other textured specimens, which reduced the wear rate by about 84%. That is the result of the equivalent reflection of the wear profile observed on this specimen.

Figure 9 shows the OM images of the wear scar developed on the counterface of the bearing steel balls. It clearly shows that the wear scar against the untextured specimen was found to have small scratches, whereas the steel balls slid against the textured specimens had visible, pronounced abrasive grooves. It showed that the grooves developed on the balls were bigger, as the roughness of the textured specimens became higher. The wear scars on the balls slid against the S80 and S100 specimens are larger than those slid against the untextured, S150 and S200 specimens. The wear scar size of the counterface balls was dependent on the roughness parameters of the contacting surfaces (rougher specimens produced larger scars on the ball). This variation in the worn surface of the balls can be correlated with the roughness of the specimens. Since the roughness of the S80 and S100 specimens was much higher, more pronounced, and visible abrasive scratches developed on the counter balls. Figure 10 presents the ball scar wear profiles mated against the untextured and textured specimens. It can be seen that the ball wear profiles mated against the S80, S100, and S150 specimens were wider and deeper compared to those of the untextured specimen. This is mainly because

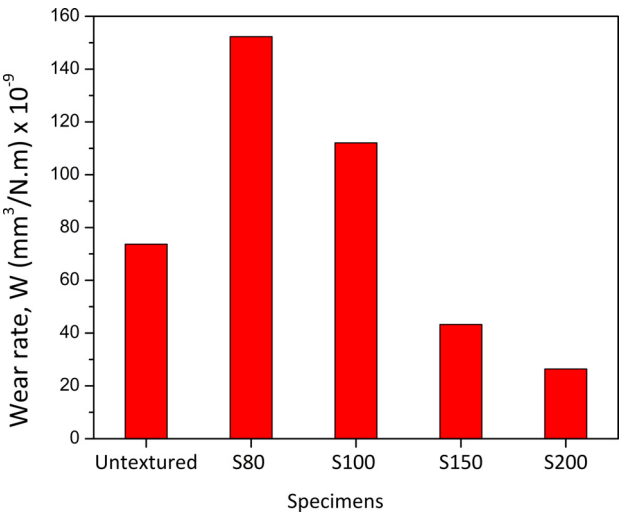

Fig. 11 Wear volume and rate of counterface balls sliding against untextured and textured specimens

of the large number of dimples lying inside the wear track for the textured specimens, which makes the surface rougher, and the higher wear of the counter balls was observed. However, the ball wear profile of the steel ball mated against the S200 specimen showed itself to be much narrower and shallower, as this specimen is comprised of a fewer number of dimples inside the contact area in comparison with the other textured specimens. The wear rates of the counter balls are presented in Fig. 11. To elucidate the wear mechanism, the wear tracks on the untextured and textured specimens were observed using a mini-SEM. The wear on all the specimens was mainly abrasive, since only abrasive grooves were visible on worn part of the specimens. Little adhesive wear was also observed followed by abrasive wear. The textured specimens automatically reduce the amount of wear because of the decrease in the contact area, which is in complete agreement with the literature on this subject. Vilhena et al. have reported no measurable wear for all the textured specimens under the investigated contact conditions [35].

Conclusions

In this study, LST was used to produce dimples (diameter = 60 μm, depth = 30 μm) with a dimple pitch of 80–200 μm. The following conclusions can be drawn from this experimental investigation:

(1) The friction coefficient of the textured specimen having a dimple density of 13% and a dimple pitch of 150 μm reduced by about 70% compared to that of the untextured specimen.
(2) The wear rate of the textured specimen having a dimple density of 7% and a dimple pitch of 200 μm decreased by about 84% compared to that of the untextured specimen, despite high surface roughness.
(3) It was found that the wear of the counterface ball was dependent on the surface roughness of the disk specimen.
(4) It was also shown that the textured specimen with a higher R_{ku} and a maximum negative R_{sk} will lead to a lower friction coefficient and lesser wear.
(5) The lowest friction coefficient was achieved at a load of 15 N within the observed range. The friction coefficient of the textured specimen reduced with increasing normal load.
(6) The friction coefficient can be reduced with increasing sliding speed.

Acknowledgment

This research was supported by the Pioneer Research Program through the National Research Foundation of Korea funded by the Ministry of Education, Science and Technology (No. 2010-0019473).

Nomenclature

d_d = diameter of dimples of textured specimens
d_w = wear scar diameter of the ball
EHL = elastohydrodynamic lubrication
f = focal length of the objective lens of laser instrument
h = height of worn part of the ball
l = total sliding distance
N = normal load
r = radius of the ball
S = dimple pitch
V = wear volume
W = wear rate

References

[1] Xiao, L., Rosen, B. G., Amini, N., and Nilsson, P. H., 2003, "A Study on the Effect of Surface Topography on Rough Friction in Roller Contact," Wear, **254**(11), pp. 1162–1169.
[2] Keller, J., Fridrici, V., Kapsa, P., and Huard, J. F., 2009, "Surface Topography and Tribology of Cast Iron in Boundary Lubrication," Tribol. Int., **42**(6), pp. 1011–1018.
[3] Hisakado, J., and Tani, H., 1999, "Effects of Elevated Temperatures and Topographies of Worn Surfaces on Friction and Wear of Ceramics in Vacuum," Wear, **224**(1), pp. 165–172.
[4] Wang, X., Adachi, K., Otsuka, K., and Kato, K., 2006, "Optimization of the Surface Texture for Silicon Carbide Sliding in Water," Appl. Surf. Sci., **253**(3), pp. 1282–1286.
[5] Schreck, S., and Zum Gahr, K. H., 2005, "Laser-Assisted Structuring of Ceramic and Steel Surfaces for Improving Tribological Properties," Appl. Surf. Sci., **247**(1–4), pp. 616–622.
[6] Wu, S.-C., Tseng, K.-H., Wen, H.-C., Wu, M.-J., and Chou, C.-P., 2013, "Tribological Behavior of Electron Beam D6ac Weldment," Appl. Surf. Sci., **264**, pp. 45–51.
[7] Borghi, A., Gualtieri, E., Marchetto, D., Moretti, L., and Valeri, S., 2008,"Tribological Effects of Surface Texturing on Nitriding Steel for High-Performance Engine Applications," Wear, **265**(7–8), pp. 1046–1051.
[8] Gao, Y., Wu, B., Zhou, Y., and Tao, S., 2011, "A Two-Step Nanosecond Laser Surface Texturing Process With Smooth Surface Finish," Appl. Surf. Sci., **257**(23), pp. 9960–9967.
[9] Garrido, A. H., González, R., Cadenas, M., and Battez, A. H., 2011, "Tribological Behavior of Laser-Textured NiCrBSi Coatings," Wear, **271**(5–6), pp. 925–933.
[10] Hu, T., Hu, L., and Ding, Q., 2012, "Effective Solution for the Tribological Problems of Ti-6Al-4V: Combination of Laser Surface Texturing and Solid Lubricant Film," Surf. Coat. Technol., **206**(24), pp. 5060–5066.
[11] Li, J., Xiong, D., Wu, H., Zhang, Y., and Qin, Y., 2013, "Tribological Properties of Laser Surface Texturing and Molybdenizing Duplex-Treated Stainless Steel at Elevated Temperatures," Surf. Coat. Technol., **228**(Suppl. 1), pp. S219–S223.
[12] Voevodin, A. A., and Zabinski, J. S., 2006, "Laser Surface Texturing for Adaptive Solid Lubrication," Wear, **261**(11–12), pp. 1285–1292.
[13] Wan, Y., and Xiong, D.-S., 2008, "The Effect of Laser Surface Texturing on Frictional Performance of Face Seal," J. Mater. Process. Technol., **197**(1–3), pp. 96–100.
[14] Wu, Z., Deng, J., Xing, Y., Cheng, H., and Zhao, J., 2012, "Effect of Surface Texturing on Friction Properties of WC/Co Cemented Carbide," Mater. Des., **41**, pp. 142–149.
[15] Vilhena, L. M., Sedlaček, M., Podgornik, B., Vižintin, J., Babnik, A., and Možina, J., 2009, "Surface Texturing by Pulsed Nd:YAG Laser," Tribol. Int., **42**(10), pp. 1496–1504.
[16] Kovalchenko, A., Ajayi, O., Erdemir, A., and Fenske, G., 2011, "Friction and Wear Behavior of Laser Textured Surface Under Lubricated Initial Point Contact," Wear, **271**(9–10), pp. 1719–1725.
[17] Amanov, A., Tsukasa, W., Ryo, T., and Shinya, S., 2013, "Improvement in the Tribological Characteristics of Si-DLC Coating by Laser Surface Texturing Under Oil-Lubricated Point Contacts at Various Temperatures," Surf. Coat. Technol., **232**, pp. 549–560.
[18] Ramesh, A., Akram, W., Mishra, S. P., Cannon, A. H., Polycarpou, A. A., and King, W. P., 2013, "Friction Characteristics of Microtextured Surfaces Under Mixed and Hydrodynamic Lubrication," Tribol. Int., **57**, pp. 170–176.
[19] Li, K., Hu, Y., and Yao, Z., 2013, "Experimental Study of Micro Dimple Fabrication Based on Laser Shock Processing," Opt. Laser Technol., **48**, pp. 216–225.
[20] Huang, W., Jiang, L., Zhou, C., and Wang, X., 2012, "The Lubricant Retaining Effect of Micro-Dimples on the Sliding Surface of PDMS," Tribol. Int., **52**, pp. 87–93.
[21] Meng, F., Zhou, R., Davis, T., Cao, J., Wang, Q. J., Hua, D., and Liu, J., 2010, "Study on Effect of Dimples on Friction of Parallel Surfaces Under Different Sliding Conditions," Appl. Surf. Sci., **256**(9), pp. 2863–2875.
[22] Etsion, I., 2013, "Modeling of Surface Texturing in Hydrodynamic Lubrication," Friction, **1**(3), pp. 195–209.
[23] Neville, A., Morina, A., Haque, T., and Voong, M., 2007, "Compatibility Between Tribological Surfaces and Lubricant Additives—How Friction and Wear Reduction Can Be Controlled by Surface/Lube Synergies," Tribol. Int., **40**(10–12), pp. 1680–1695.
[24] Kovalchenko, A., Ajayi, O., Erdemir, A., Fenske, G., and Etsion, I., 2005, "The Effect of Laser Surface Texturing on Transitions in Lubrication Regimes During Unidirectional Sliding Contact," Tribol. Int., **38**(3), pp. 219–225.
[25] Yan, D., Qu, N., Li, H., and Wang, X., 2010, "Significance of Dimple Parameters on the Friction of Sliding Surfaces Investigated by Orthogonal Experiments", Tribol. Trans., **53**(5), pp. 703–712.
[26] Galda, L., Pawlus, P., and Sep, J., 2009, "Dimples Shape and Distribution Effect on Characteristics of Stribeck Curve," Tribol. Int., **42**(10), pp. 1505–1512.
[27] Jianliang Li, J., and Xiong, D., 2009, "Tribological Behavior of Graphite-Containing Nickel-Based as Function of Temperature, Load and Counterface," Wear, **266**(1–2), pp. 360–367.
[28] Petropoulos, G. P., Pandazaras, N. C., and Davim, J. P., 2010, *Surface Integrity in Machining*, Springer, London, pp. 37–66.
[29] Sedlaček, M., Podgornik, B., and Vižintin, J., 2009, "Influence of Surface Preparation on Roughness Parameters, Friction and Wear," Wear, **266**(3–4), pp. 482–487.
[30] Podgornik, B., Vilhena, L. M., Sedlaček, M., Rek, Z., and Žun, I., 2012, "Effectiveness and Design of Surface Texturing for Different Lubrication Regimes," Meccanica, **47**(7), pp. 1613–1622.

[31] Podgornik, B., and Sedlacek, M., 2012, "Performance, Characterization and Design of Textured Surfaces," ASME J. Tribol., **134**(4), p. 041701.
[32] Kovalchenko, A., Ajayi, O., Erdemir, A., Fenske, G., and Etsion, I., 2004, "The Effect of Laser Texturing of Steel Surfaces and Speed-Load Parameters on the Transition of Lubrication Regime From Boundary to Hydrodynamic," Tribol. Trans., **47**(2), pp. 299–307.
[33] Chowdhury, M. A., Khalil, M. K., Nuruzzaman, D. M., and Rahaman, M. L., 2011, "The Effect of Sliding Speed and Normal Load on Friction and Wear Property of Aluminium," Int. J. Mech. Mechatronics Eng., **11**(1), pp. 45–49.
[34] Al-Samarai, R. A., Haftirman, Ahmed, K. R., and Al-Douri, Y., 2012, "Effect of Load and Sliding Speed on Wear and Friction of Aluminum–Silicon Casting Alloy," Int. J. Sci. Res. Publ., **2**(3), pp. 1–4.
[35] Vilhena, L. M., Podgornik, B., Vižintin, J., and Možina, J., 2011, "Influence of Texturing Parameters and Contact Conditions on Tribological Behaviour of Laser Textured Surfaces," Meccanica, **46**(3), pp. 567–575.